A multi-layered shallow water model for sediment transport in flows over heterogeneous erodible beds

Thomas Rowan* Mohammed Seaid†

Abstract

A fast and accurate finite volume method for multi-layered shallow water flows with mass exchange over erodible beds is developed. The governing equations consist of the multi-layered shallow water equations for the hydraulic variables, a set of transport equations for the suspended sediments in each layer, and a class of empirical equations for erosion and deposition effects. Mass exchange terms between layers are accounted for in both water flow and suspended sediments along with terms for sedimentary diffusion. The coupled models for each layer have been reformulated as a coupled system of conservation laws with source terms, and a two-step finite volume method is presented for its numerical solution. The method is simple, fast and second-order accurate. In the first step, the governing equations are rewritten in a non-conservative form and the numerical fluxes are calculated using the method of characteristics. In the second stage, the numerical solutions are updated in a conservative form using the finite volume discretization. Entrainment, deposition and diffusion rates are evaluated in the first stage of a splitting operator. Numerical results are presented for a multi-layered dam-break problem over an erodible bed and also for a wind-driven recirculation problem over an erodible non-flat bed. The obtained results for these examples demonstrate the capabilities of the combined multi-layered model and the finite volume method to accurately simulate shallow water flows with suspended sediments over erodible beds.

Keywords. Multi-layered shallow water flows; Finite volume method; Method of characteristics; Sediment transport; Erosion and deposition; Erodible beds

1 Introduction

The well-established Navier-Stokes equations have been widely used in the literature to model and to provide correct solutions for fluid dynamics. However, using this full three-dimensional approach is computationally demanding, thus all savings in complexity are to be welcomed in this field of research, see [20] and further references are therein. This has given rise to an extensive range of more efficient models including multi-layered shallow water models. Two classes of multi-layered models have been developed over the last decades: one in which the layers of separate fluids are immiscible, see for example [14], while the other class is based on a single fluid and allows for exchange between the layers, see for instance [2, 1, 12]. The advantage of both models is that they avoid the massive computations associated with solving the Navier-Stokes equations and at the same time, obtain stratified horizontal velocities. The shallow water equations can be derived from the non-stationary three-dimensional Navier-Stokes equations as the ratio between the vertical and horizontal scales is appropriate, correct boundary conditions are applied, and the hydrostatic pressure assumption is valid, see for example [2, 12].

*Department of Civil and Environmental Engineering, Imperial College London, South Kensington Campus, London SW72AZ, UK *E-mail:* t.rowan@imperial.ac.uk

†Department of Engineering, University of Durham, South Road, Durham DH1 3LE, UK *E-mail:* m.seaid@durham.ac.uk

In the above references, the multi-layered models have been used for shallow water flows over fixed beds only. However, the morphological and sediment transport problems are crucial to the understanding of shallow water flows in many applications. Examples of these applications include, among others, beach profile changes due to severe wave climates, seabed response to dredging procedures or imposed structures and harbor siltation. A large amount of work has been done on the effects of water flows on sediment beds, see for example [23, 30, 27, 3]. Almost all models rely on the experimental data sets for sediments that form the basis of a set of empirical formulae to be used for modeling sediment transport, see [24] among others. Many methods for modeling sediment transport exist ranging from particle tracking [9] to sediment balance software such as ESTMORPH [31]. It should be stressed that the ESTMORPH and other equilibrium-based models are computationally limited as they do not have any direct representation of the dynamics involved, while more accurate relation-driven models as those investigated in [23, 30, 27, 3] are computationally demanding. Therefore, to enable the uptake of more accurate models, highly efficient models are needed when modelling complex sediment-flow interactions. In the current study, we develop a novel multi-layered model to incorporate both movable beds and transport of sediments in shallow water flows. The governing equations consist of the multi-layered shallow water equations coupled to a set of transport equations for the suspended sediments in each layer, and a series of empirical equations for erosion and deposition terms. The interaction between the layers is accounted for through mass exchange terms in both the water flow and the sediment concentrations. In the proposed model, the presence of multiple layers in the flow systems allows for the sediment concentration to vary vertically within the water depth. In comparison to the models investigated in [16, 26] for the vertical concentration, the proposed multi-layered model can handle multiple concentrations in the system without relying on the computationally demanding vertical discretization. Recently, this has been extended to account for turbulent kinetic energy in [33]. The focus in the present work is on developing a framework within which empirical or semi-empirical relations as those reported in [33] can be easily incorporated into the numerical model as required. For bed-load and suspended sediments, we use the equations proposed in [5] but other equations as those published in [10, 17, 13, 21] can also be included in our model without major conceptual modifications.

Developing numerical solvers for the multi-layered shallow water equations often presents difficulties due to a combination of their nonlinear form, the presence of source terms, the coupling between the free-surface equation and the equations governing the water flow, compare [2, 1] among others. Including equations for bed-load and suspended sediments in the multi-layered model will add more challenges for the design of robust methods for the numerical solution of the fully coupled system. Here, the difficulty in these models comes from the coupling terms, involving some derivatives of the unknown physical variables that make the system non-conservative and possibly non-hyperbolic. Due to these terms, a numerical method originally designed for the multi-layered shallow water equations over fixed beds will lead to instabilities when it is applied to each layer separately. In the present work, we consider the Finite Volume Characteristics (FVC) method introduced in [4] for solving single-layered shallow water equations. The FVC method is second-order accurate and it avoids the solution of Riemann problems and it belongs to the predictor-corrector type methods. The predictor stage uses the method of characteristics to reconstruct the numerical fluxes, whereas the corrector stage recovers the conservation equations using the finite volume discretization. The FVC method has also been used in [1, 22] to solve a class of multi-layered shallow water equations. Based on the results reported in these references, the FVC method is simple, conservative, non-oscillatory and suitable for multi-layered shallow water flows over erodible beds for which Riemann problems are difficult or impossible to solve. In this study, improvements to the FVC method have also been made including (i) a second-order splitting operators is used for the treatment of the source terms, (ii) a third-order Runge-Kutta scheme is implemented for the time integration, and (iii) a cubic Spline interpolation is used in the predictor stage. Numerical examples are presented to verify the considered multi-layered shallow water flows over erodible beds. We demonstrate the capability of the proposed model for calculating lateral and vertical distributions of velocities for multi-layered shallow water flows over erodible flat and non-flat beds.

This paper is structured as follows. In Section 2, we introduce the models for multi-layered shallow water flows over erodible beds. The finite volume characteristics method for solving the governing equations is presented in Section 3. This section includes the reconstruction of the numerical fluxes using the modified method of characteristics and the discretization of the source terms in the model. In Section 4, we examine the numerical performance of the proposed models using two test examples. We present numerical results for both a dam-break flow and for a wind-driven flow over erodible beds. Concluding remarks and recommendations for future work are given in Section 5.

2 Equations for multi-layered shallow water flows over erodible beds

Multi-layered flow systems are mainly obtained using a vertical discretization of the three-dimensional Navier-Stokes equations accounting for the shallow water assumptions, compare [1, 2] and further references are therein. In the present study, we consider the one-dimensional version of the model for each of the layers of fluid and it includes equations for sediment transport, terms for mass exchange between the layers and terms for the forces between the erodible bed and the water flow. Thus, in a multi-layered system of a total number of M layers, the shallow water equations for each layer $k = 1, 2, \ldots, M$ read as

$$\begin{aligned} \frac{\partial h_k}{\partial t} + \frac{\partial \left(h_k u_k\right)}{\partial x} &= G_{k-1/2} - G_{k+1/2}, \\ \frac{\partial \left(h_k u_k\right)}{\partial t} + \frac{\partial}{\partial x}\left(h_k u_k^2 + \frac{1}{2l_k} g h_k^2\right) &= -g h_k \frac{\partial B}{\partial x} + F_k, \end{aligned} \tag{1}$$

where $u_k(t,x)$ is the depth-averaged water velocity of the kth layer, $B(t,x)$ the bottom topography, g the gravitational acceleration, and $h_k(t,x)$ the water height of the kth layer defined as

$$h_k = l_k H, \qquad k = 1, \ldots, M, \tag{2}$$

where $H(t,x)$ is the total water depth and l_k is the proportional height of the kth layer in the flow system, see Figure 1 for an illustration. In (1), F_k includes the inter-layer forces and it is defined below, and $G_{k\pm1/2}$ are mass exchange terms between the layers including erosion and deposition in the lower layer as

$$G_{k-1/2} = \begin{cases} \displaystyle\sum_{i=1}^{k} \left(\frac{\partial \left(h_i u_i\right)}{\partial x} - l_i \sum_{j=1}^{M} \frac{\partial \left(h_j u_j\right)}{\partial x} \right) + \frac{E_k - D_k}{1-p}, & \text{if} \quad k = 2, 3, \ldots, M, \\ \dfrac{E_1 - D_1}{1-p}, & \text{if} \quad k = 1, \end{cases} \tag{3}$$

with E_k and D_k represent the entrainment and deposition terms in the upward and downward directions, respectively. Following the same procedure as in [2], we sum over all layers in the first equation in (1) to obtain a single equation to the total water height H as

$$\frac{\partial H}{\partial t} + \sum_{j=1}^{M} \frac{\partial \left(h_j u_j\right)}{\partial x} = \frac{E_1 - D_1}{1-p}.$$

In the current study, we also consider bed-load and suspended sediments within the multi-layered shallow water system (1). To this end, we define the depth-averaged concentration c_k for the kth layer as

$$c_k = \frac{\rho_k - \rho_w}{\rho_s - \rho_w}, \tag{4}$$

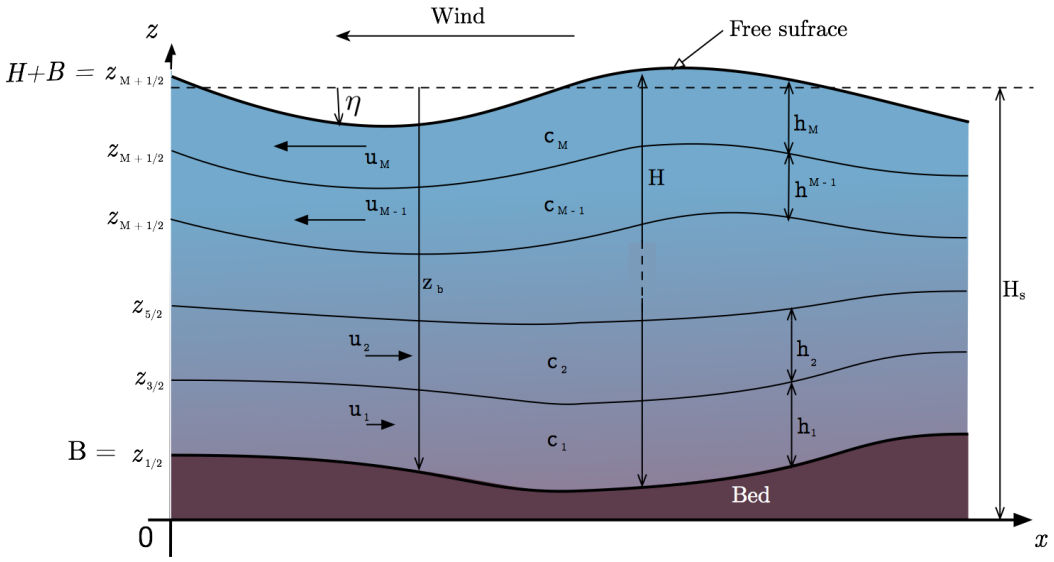

Figure 1: A simple illustration of multi-layered shallow water flows over erodible beds. Each layer k ($k = 1, 2, \ldots, M$) is characterized with a water height h_k, a water velocity u_k, and a sediment concentration c_k. The initial bed is denoted by B.

where p is the porosity, ρ_w the water density, ρ_s the sediment density and ρ_k is the density of the water-sediment mixture in the kth layer. Here, the density of the saturated bed ρ_0 is related to the porosity as

$$\rho_0 = \rho_w p + \rho_s (1 - p).$$

Hence, the governing equations we consider for modeling multi-layered shallow water flows over erodible beds are

$$\begin{aligned}
\frac{\partial H}{\partial t} + \sum_{k=1}^{M} \frac{\partial (h_k u_k)}{\partial x} &= \frac{E_1 - D_1}{1-p}, \\
\frac{\partial (h_k u_k)}{\partial t} + \frac{\partial}{\partial x}\left(h_k u_k^2 + \frac{1}{2} g h_k H \right) &= -g h_k \frac{\partial B}{\partial x} - \frac{(\rho_s - \rho_w)}{2\rho_k} g h_k^2 \frac{\partial c_k}{\partial x} + F_k, \\
\frac{\partial (h_k c_k)}{\partial t} + \frac{\partial}{\partial x}\left(h_k u_k c_k \right) &= E_k - D_k + c_{k+1/2} G_{k+1/2} - c_{k-1/2} G_{k-1/2} + \\
&\quad \varepsilon_c \left(\frac{\partial^2 c_{\Delta,k-1/2}}{\partial z^2} - \frac{\partial^2 c_{\Delta,k+1/2}}{\partial z^2} \right), \\
\frac{\partial B}{\partial t} &= -\frac{E_1 - D_1}{1-p},
\end{aligned} \tag{5}$$

where E_1 and D_1 are the erosion and deposition rates on the bottom fluid layer, respectively. In this study, the inter-layer diffusion in the concentration is handled by considering the diffusion potential between two layers $c_{\Delta,k-1/2}$ and $c_{\Delta,k+1/2}$ and a diffusion coefficient ε_c. Note that these terms are included in the model to handle the sediment diffusion. In (5), the external force F_k acting on the kth layer accounting for friction and momentum exchange effects is given by

$$F_k = F_k^{(u)} + F_k^{(b)} + F_k^{(w)} + F_k^{(\mu)}, \tag{6}$$

with $F_k^{(u)}$ is related to the momentum exchanges between the layers and defined as

$$\begin{aligned} F_k^{(u)} &= u_{k+1/2}G_{k+1/2} - u_{k-1/2}G_{k-1/2} - \frac{1}{l_k}\frac{(\rho_0-\rho_k)(E_k-D_k)u_k}{\rho_k(1-p)} - \\ &\quad \frac{(\rho_s-\rho_w)}{2\rho_k}gh_k^2\left(\varepsilon_c\frac{\partial^2 c_{\Delta,k-1/2}}{\partial z^2} - \varepsilon_c\frac{\partial^2 c_{\Delta,k+1/2}}{\partial z^2} + c_{k+1/2}G_{k+1/2} - c_{k-1/2}G_{k-1/2}\right), \end{aligned}$$

where $c_{\Delta,k-1/2}$ is the concentration of diffusible material at each layer interface defined below. Here, the intermediate velocity $u_{k+1/2}$ and concentration $c_{k+1/2}$ are reconstructed using an upwind method based on the sign of the mass exchange term as

$$u_{k+1/2} = \begin{cases} u_k, & \text{if} \quad G_{k+1/2} \geq 0, \\ u_{k+1}, & \text{otherwise}, \end{cases} \qquad c_{k+1/2} = \begin{cases} c_k, & \text{if} \quad G_{k+1/2} \geq 0, \\ c_{k+1}, & \text{otherwise}. \end{cases}$$

The vertical kinematic eddy viscosity term $F_k^{(\mu)}$ in (6) takes into account the friction between neighboring layers as

$$F_k^{(\mu)} = \begin{cases} -2\nu\dfrac{u_{k-1}-u_k}{(l_{k-1}+l_k)H}, & \text{if} \quad k = M, \\ 2\nu\dfrac{u_{k+1}-u_k}{(l_{k+1}+l_k)H} - 2\nu\dfrac{u_{l-1}-u_k}{(l_{k-1}+l_k)H}, & \text{if} \quad k = 2,\ldots,M-1, \\ 2\nu\dfrac{u_{l+1}-u_k}{(l_{k+1}+l_k)H}, & \text{if} \quad k = 1, \end{cases}$$

where ν is the eddy viscosity. The external bed friction term $F_k^{(b)}$ in (6) is given as

$$F_k^{(b)} = \begin{cases} -\dfrac{gn_b^2}{H^{1/3}}u_1|u_1|, & \text{if} \quad k = 1, \\ 0, & \text{otherwise}, \end{cases}$$

where n_b is the Manning roughness coefficient. The surface wind force $F_k^{(w)}$ in (6) is defined as

$$F_k^{(w)} = \begin{cases} -\dfrac{\sigma^2\rho_a}{H}\left(w-u_k\right)\left|w-u_k\right|, & \text{if} \quad k = M, \\ 0, & \text{otherwise}, \end{cases}$$

where w is the wind velocity at 10 m above the water surface, ρ_a the air density and σ is the wind stress coefficient. Note that for the bottom layer, an equation that relates the effects of an erodible bed is included in the model (5). These equations are presented in a general form such that appropriate erosion and deposition equations can be substituted with ease. Thus, to determine the entrainment and deposition terms in (5), the empirical relations reported in [5] are used as

$$D_k = \begin{cases} w_s\left(1-c_B\right)^m c_B, & \text{if} \quad k = 1, \\ 0, & \text{otherwise}, \end{cases} \tag{7}$$

where w_s is the deposition coefficient experimentally measured in [28, 32, 24], d the averaged diameter of the sediment particles, m an exponent indicating the effects of hindered settling due to high sediment

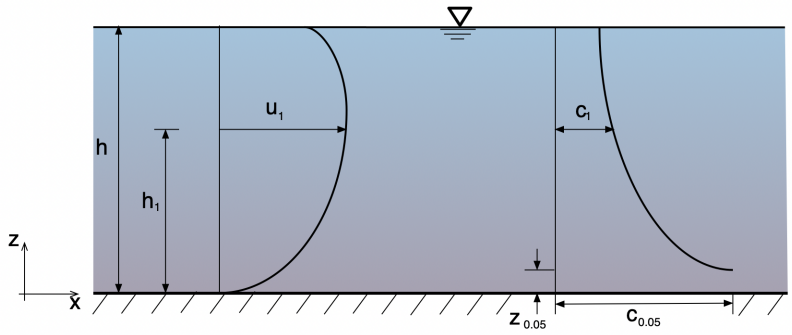

Figure 2: Typical sediment distribution in a flow system adapted from [19]. Here, we illustrate the velocity distribution u and the concentration distribution C_0 as functions of the water depth h with a maximum concentration $c_{0.05}$ at $z_{0.05}$.

concentrations and set to $m = 2$. In the current study, we use empirical values for the settling velocity w_s calculated based on the following equation

$$w_s = \frac{\sqrt{(36\nu/d)^2 + 7.5\rho_s g d} - 36\nu/d}{2.8},$$

where ν is the kinematic viscosity of water. Note that more developed empirical equations for the settling velocity as those studied in [28] can also be used in the proposed model.

In (7), $c_B = \beta_c c_k$ is the near-bed volumetric sediment concentration, and $c_\Delta = \beta_c(c_k - c_{k-1})$ is the concentration for inter-layer settling. Here, β_{c_k} is a coefficient larger than unity used to ensure that the near-bed concentration does not exceed $(1-p)$ and it is defined in [6] by

$$\beta_{c_k} = \min\left(2, \frac{1-p}{c_k}\right).$$

For the entrainment of the material the following relation is used [6]

$$E_k = \begin{cases} \varphi \dfrac{\theta - \theta_{cr}}{h_1} u_1 d^{-0.2}, & \text{if} \quad \theta \geq \theta_{cr} \quad \text{and} \quad k = 1, \\ 0, & \text{otherwise}, \end{cases} \tag{8}$$

where φ is a coefficient to control the erosion forces, that is empirical, θ_{cr} is a critical value of Shields parameter for the initialization of sediment motion and θ is the Shields coefficient defined by

$$\theta = \frac{u_*^2}{sgd},$$

with $s = \frac{\rho_s}{\rho_w} - 1$ is the submerged specific gravity of sediment and u_* is the friction velocity defined as

$$u_*^2 = \sqrt{\frac{g\, n_b^2}{h^{1/3}}} \left|u_1\right|.$$

Note that the equations used for the entrainment and deposition have been widely used in the literature for the conventional single-layered shallow water flows over erodible beds, see for example [28, 32, 24, 3]. It should also be pointed out that no vertical velocities are calculated in the proposed model, but the vertical sediment diffusion is a major problem for a formulation of this type. In this

study, a sediment diffusion coefficient ε_c is introduced in the multi-layered model (5). Research has also been undertaken in experimental [29] and in computational [15, 16] studies to model the vertical diffusion of sediment in water flows and Figure 2 shows a typical sediment distribution in a flow system. As the shape, size, and precise distribution for various sediment types have been categorized, a simplistic method for the vertical distribution is proposed here and it is shown in Figure 2. This model is based on the study reported in [19] and it is used in the present study as it is interchangeable for a variety of sediment models and it also helps to describe slower bed flow as well as faster suspended flows. Calculating the diffusion for each cell boundary is computationally demanding, consequently a distribution curve for the quantity of diffusion is implemented. The curve is calculated by comparing the sediment to be diffused to the portion that should be diffused, for example $C_0 = \dfrac{1}{h}$. Then, by applying limits for each layer, the curve yields

$$C_{0,k} = \left(\frac{\ln(z_{k+\frac{1}{2}}) - \ln(z_{k-\frac{1}{2}})}{\ln(h+\lambda_c) - \ln(h_{0.05}+\lambda_c)} \right) \sum_{k=1}^{M} (c_k h_k)\,,$$

where z_k is the depth of the kth layer, $h_{0.05}$ the effective bottom (*i.e.* where the bed-load takes over) and λ_c an empirically measured coefficient used to describe the concentration curve. Hence, the concentration of diffusible material at each layer interface is defined as

$$\frac{\partial^2 c_{\Delta,k+\frac{1}{2}}}{\partial z^2} = \frac{C_{0,k+1} - c_{k+1}h_{k+1} - C_{0,k} + c_k h_k}{h_k}, \qquad \text{for} \quad k = 1, 2, \ldots, M-1.$$

Note that this method can easily be adapted to any sediment distribution curve and, as the distribution curve can be calculated in advance of any time-stepping procedure, it is highly efficient. For instance, the curves discussed in [33] can also be used in our model without major modifications.

For ease of presentation, we re-arrange the governing equations (5) into a compact vector form as

$$\frac{\partial \mathbf{W}}{\partial t} + \frac{\partial \mathbf{F}(\mathbf{W})}{\partial x} = \mathbf{Q}(\mathbf{W}) + \mathbf{R}(\mathbf{W}), \tag{9}$$

where $\mathbf{W}$ is the vector of conserved variables, $\mathbf{F}(\mathbf{W})$ is the vector of flux functions, $\mathbf{Q}(\mathbf{W})$ and $\mathbf{R}(\mathbf{W})$ are the vectors of source terms defined by

$$\mathbf{W} = \begin{pmatrix} H \\ Hu_1 \\ Hc_1 \\ Hu_2 \\ Hc_2 \\ \vdots \\ Hu_k \\ Hc_k \\ B \end{pmatrix}, \; \mathbf{F}(\mathbf{W}) = \begin{pmatrix} \sum_{\alpha=1}^{k} l_\alpha H u_\alpha \\ Hu_1^2 + \frac{1}{2}gH^2 \\ Hu_1 c_1 \\ Hu_2^2 + \frac{1}{2}gH^2 \\ Hu_2 c_2 \\ \vdots \\ Hu_k^2 + \frac{1}{2}gH^2 \\ Hu_k c_k \\ 0 \end{pmatrix}, \; \mathbf{Q}(\mathbf{W}) = \begin{pmatrix} 0 \\ -gH\frac{\partial B}{\partial x} - \frac{(\rho_s-\rho_w)}{2\rho_1} g l_1 H^2 \frac{\partial c_1}{\partial x} \\ 0 \\ -gH\frac{\partial B}{\partial x} - \frac{(\rho_s-\rho_w)}{2\rho_2} g l_2 H^2 \frac{\partial c_2}{\partial x} \\ 0 \\ \vdots \\ -gH\frac{\partial B}{\partial x} - \frac{(\rho_s-\rho_w)}{2\rho_k} g l_M H^2 \frac{\partial c_k}{\partial x} \\ 0 \\ 0 \end{pmatrix},$$

$$\mathbf{R}(\mathrm{W}) = \begin{pmatrix} \dfrac{E_1 - D_1}{1-p} \\ -\dfrac{1}{l_1}\left(F_1^{(u)} + F_1^{(b)} + F_1^{(\mu)}\right) \\ E_1 - D_1 - G_{3/2}c_{3/2} - \varepsilon_c \dfrac{\partial^2 c_{\Delta,3/2}}{\partial z^2} \\ -\dfrac{1}{l_2}\left(F_2^{(u)} + F_2^{(\mu)}\right) \\ +G_{5/2}c_{5/2} - G_{3/2}c_{3/2} + \varepsilon_c \dfrac{\partial^2 c_{\Delta,3/2}}{\partial z^2} - \varepsilon_c \dfrac{\partial^2 c_{\Delta,5/2}}{\partial z^2} \\ \vdots \\ -\dfrac{1}{l_k}\left(F_k^{(u)} + F_k^{(w)} + F_k^{(\mu)}\right) \\ -G_{M-1/2}c_{M-1/2} + \varepsilon_c \dfrac{\partial^2 c_{\Delta,M-1/2}}{\partial z^2} \\ -\dfrac{E_1 - D_1}{1-p} \end{pmatrix}. \tag{10}$$

It should be stressed that the source term $\mathbf{Q}$ contains the first-order differential terms with respect to the coordinate x, while the remaining forces are included in the source term $\mathbf{R}$. This structure is advantageous as it allows for a time splitting operator in (9), for which the source terms $\mathbf{Q}$ and $\mathbf{R}$ are treated separately in different stages of the splitting.

3 A Fast finite Volume Method of Characteristics

To integrate the system (9) in time, we divide the time interval into subintervals $[t_n, t_{n+1}]$ with length $\Delta t = t_{n+1} - t_n$ and we use the notation W^n to denote the value of a generic function W at time t_n. Here, we use the second-order order splitting procedure [34] carried out in three stages as:

Stage 1: Solve for $\mathbf{W}^*$

$$\begin{aligned} \frac{\partial \mathbf{W}^*}{\partial t} &= \mathbf{R}(\mathbf{W}^*), \qquad t \in (t_n, t_{n+1/2}], \\ \mathbf{W}^*(t_n) &= \mathbf{W}(t_n). \end{aligned} \tag{11}$$

Stage 2: Solve for $\mathbf{W}^{**}$

$$\begin{aligned} \frac{\partial \mathbf{W}^{**}}{\partial t} + \frac{\partial \mathbf{F}(\mathbf{W}^{**})}{\partial x} &= \mathbf{Q}(\mathbf{W}^{**}), \qquad t \in (t_n, t_{n+1}], \\ \mathbf{W}^{**}(t_n) &= \mathbf{W}^*(t_{n+1/2}). \end{aligned} \tag{12}$$

Stage 3: Solve for $\mathbf{W}^{***}$

$$\begin{aligned} \frac{\partial \mathbf{W}^{***}}{\partial t} &= \mathbf{R}(\mathbf{W}^{***}), \qquad t \in (t_{n+1/2}, t_{n+1}], \\ \mathbf{W}^{***}(t_{n+1/2}) &= \mathbf{W}^{**}(t_{n+1}). \end{aligned} \tag{13}$$

To complete the time integration, the explicit third-order Runge-Kutta method [25] is used for each stage in (11)-(13). For instance, to advance the solution of (11) from time t_n to the next time t_{n+1} we use

$$\begin{aligned} \mathcal{W}^{(1)} &= \mathbf{W}^n + \Delta t \mathbf{R}(\mathbf{W}^n), \\ \mathcal{W}^{(2)} &= \frac{3}{4}\mathbf{W}^n + \frac{1}{4}\mathcal{W}^{(1)} + \frac{1}{4}\Delta t \mathbf{R}(\mathcal{W}^{(1)}), \\ \mathbf{W}^{n+1} &= \frac{1}{3}\mathbf{W}^n + \frac{2}{3}\mathcal{W}^{(2)} + \frac{2}{3}\Delta t \mathbf{R}(\mathcal{W}^{(2)}), \end{aligned} \tag{14}$$

where we have dropped the asterisk of the variables for ease in the notation. Note that the Runge-Kutta method (14) is TVD, third-order accurate in time, and stable under the usual Courant-Friedrichs-Lewy (CFL) condition involving eigenvalues of the system under study. Note that explicit expressions of the eigenvalues for the system (9) are not trivial to find and as for multi-layered shallow water equation over fixed beds there may exist situations for which eigenvalues become complex. In these cases, the multi-layered system (9) is not hyperbolic and yields to the so-called Miles-Howard instability at the water interfaces [8]. As a consequence, most finite volume methods which are based on Riemann solvers would fail to resolve the system (9) for the multi-layered shallow water equations over erodible beds. In the present study, we consider the Finite Volume Method of Characteristics (FVC) method introduced in [4] and used in [1] for the numerical solution of multi-layered shallow water flows over fixed beds. In this section, we briefly describe the FVC formulation for the system (9) and further details can be found in [4, 1]. Note that the FVC method does not require the calculation of the eigenvalues for the multi-layered system (5). However, the selection of time steps is carried out using the eigenvalues associated with the single-layered counterpart of the system (5) which are defined in [3] as

$$\lambda_1 = 0, \quad \lambda_{2,k} = u_k, \quad \lambda_{3,k} = u_k - \sqrt{gh_k}, \quad \lambda_{4,k} = u_k + \sqrt{gh_k}, \qquad k = 1, 2 \ldots, M. \tag{15}$$

Note that the eigenvalues (15) are for the single-layered sediment transport system associated with (5) using the water heights h_k and not the total height H. This results in a system of $(3M+1)$ equations for which each uncoupled layer, its associated four eigenvalues are given by (15). It should also be stressed that similar approach has been considered in [1] for multi-layered shallow water flows over fixed beds for which eigenvalues of it single-layered counterpart have been used in the simulations.

3.1 Discretization of the flux gradients and source terms

Let us discretize the spatial domain into control volumes $[x_{i-1/2}, x_{i+1/2}]$ centered at x_i with a step size Δx. For the space discretization of the equations (9), we use the notations

$$\mathbf{W}_{i\pm\frac{1}{2}}(t) = \mathbf{W}(t, x_{i\pm\frac{1}{2}}) \quad \text{and} \quad \mathbf{W}_i(t) = \frac{1}{\Delta x}\int_{x_{i-\frac{1}{2}}}^{x_{i+\frac{1}{2}}} \mathbf{W}(t,x)dx,$$

to denote the point-values and the approximate cell-average of the variable $\mathbf{W}$ at the gridpoint $(t, x_{i\pm\frac{1}{2}})$ and (t, x_i), respectively. Integrating the equation (12) with respect to space over the control volume, we obtain the following semi-discrete equation

$$\frac{d\mathbf{W}_i}{dt} + \frac{\mathbf{F}_{i+1/2} - \mathbf{F}_{i-1/2}}{\Delta x} = \mathbf{Q}_i, \tag{16}$$

where $\mathbf{F}_{i\pm1/2} = \mathbf{F}(\mathbf{W}_{i\pm1/2})$ are the numerical fluxes at the cell interfaces $x = x_{i\pm1/2}$. In (16), $\mathbf{Q}_i$ is a consistent discretization of the source term $\mathbf{Q}$ in (9). To reconstruct the numerical fluxes $\mathbf{F}_{i\mp1/2}$ we consider the method of characteristics applied to the advective version of the system (12). Without accounting for the source term $\mathbf{R}(\mathbf{W})$ we reformulate the equations in (5) into the advective form

$$\begin{aligned}
\frac{\partial H}{\partial t} + \left(\sum_{j=1}^{M} l_j u_j\right)\frac{\partial H}{\partial x} &= -\sum_{j=1}^{M} l_j H \frac{\partial u_j}{\partial x}, \\
\frac{\partial Q_k}{\partial t} + u_k\frac{\partial Q_k}{\partial x} &= -Q_k\frac{\partial u_k}{\partial x} - gH\frac{\partial (H+B)}{\partial x} - \frac{(\rho_s-\rho_w)}{2\rho_k} g l_k H^2 \frac{\partial c_k}{\partial x}, \\
\frac{\partial P_k}{\partial t} + u_k\frac{\partial P_k}{\partial x} &= -P_k\frac{\partial u_k}{\partial x},
\end{aligned} \tag{17}$$

where the discharge $Q_k = Hu_k$ and the sediment remittance $P_k = Hc_k$. The system (17) can also be rearranged in a compact form as

$$\frac{D_k U_k}{Dt} = S_k\left(\mathbf{U}\right), \qquad k = 0, 1, 2, \ldots, 2M, \tag{18}$$

with $\frac{D_k}{Dt}$ is the total derivative defined by

$$\frac{D_k}{Dt} = \frac{\partial}{\partial t} + \mathcal{U}_k \frac{\partial}{\partial x}, \qquad k = 0, 1, 2, \ldots, 2M, \tag{19}$$

where $\mathbf{U} = (U_0, U_1, \ldots, U_{2M})^T$, $\mathbf{S}\left(\mathbf{U}\right) = (S_0, S_1, \ldots, S_{2M})^T$ with

$$\mathbf{U} = \begin{pmatrix} H \\ Q_1 \\ P_1 \\ \vdots \\ Q_M \\ P_M \end{pmatrix}, \qquad \mathbf{S}(\mathbf{U}) = \begin{pmatrix} -\sum_{j=1}^{M} l_j H \frac{\partial u_j}{\partial x} \\ -Q_1 \frac{\partial u_1}{\partial x} - gH \frac{\partial\left(H+B\right)}{\partial x} - \frac{(\rho_s - \rho_w)}{2\rho_1} g l_1 H^2 \frac{\partial c_1}{\partial x} \\ -P_1 \frac{\partial u_1}{\partial x} \\ \vdots \\ -Hu_M \frac{\partial u_M}{\partial x} - gH \frac{\partial\left(H+B\right)}{\partial x} - \frac{(\rho_s - \rho_w)}{2\rho_M} g l_M H^2 \frac{\partial c_M}{\partial x} \\ -P_M \frac{\partial u_M}{\partial x} \end{pmatrix},$$

and the advection velocity $\mathcal{U}_k$ is defined as

$$\mathcal{U}_k = \begin{cases} \sum_{j=1}^{M} l_j u_j, & \text{if} \quad k = 0, \\ u_{\frac{k+1}{2}}, & \text{if} \quad k = 1, 3, 5, \ldots, \\ u_{\frac{k}{2}}, & \text{if} \quad k = 2, 4, 6, \ldots. \end{cases} \tag{20}$$

Note that we used $k = 0$ in the above equations to only formulate the compact advective form (18) for all the equations and it does not refer to any layer in the system. The principal idea of the FVC method is to use the method of characteristics to approximate the numerical fluxes in (16). Hence, the characteristic curves associated with the system (18) are solutions of the initial-value problems

$$\begin{aligned} \frac{dX_{k,i+1/2}(\tau)}{d\tau} &= \mathcal{U}_{k,i+1/2}\Big(\tau, X_{k,i+1/2}(\tau)\Big), \quad \tau \in [t_n, t_{n+1}], \\ X_{k,i+1/2}(t_{n+1}) &= x_{i+1/2}, \qquad k = 0, 1, \ldots, 2M. \end{aligned} \tag{21}$$

Here, $X_{k,i+1/2}(\tau)$ are the departure points at time τ of a particle that will arrive at the interface gridpoint $x_{i+1/2}$ in time t_{n+1}. Notice that unlike the Lagrangian methods, the method of characteristics does not follow the flow particles forward in time, but it traces backward the position at time t_n of flow particles that will reach the fixed gridpoints at time t_{n+1}. To solve the system of ordinary differential equations (21) we employ the third-order Runge-Kutta scheme (14). It should be noted that only second-order approximations for (21) has been used in [4, 1].

Once the characteristics curves $X_{k,i+1/2}(t_n)$ in (21) are calculated, a solution at the cell interface $x_{i+1/2}$ is approximated as

$$U^{n+1}_{k,i+1/2} := U_k\left(t_{n+1}, x_{i+1/2}\right) = \widetilde{U}_k\left(t_n, X_{k,i+1/2}(t_n)\right), \tag{22}$$

where $\widetilde{U}_k\left(t_n, X_{k,i+1/2}(t_n)\right)$ is the solution at the departure point $X_{k,i+1/2}(t_n)$ approximated by interpolation either globally or locally using the gridpoints of the control volume where it belongs *i.e.*

$$\widetilde{U}_k\left(t_n, X_{k,i+1/2}(t_n)\right) = \mathcal{P}\Big(U_k\left(t_n, X_{k,i+1/2}(t_n)\right)\Big), \tag{23}$$

where $\mathcal{P}$ represents an interpolating operator. Authors in [4, 1] used the Lagrange interpolation polynomials in (23). In the current work, we use the cubic Spline interpolation to approximate the solutions at the characteristics points. Other high-order interpolation procedures can also be applied.

In what follows we use the first-order Euler scheme to illustrate the formulation of the FVC method but in all our simulations the third-order Runge-Kutta scheme (14) is used. Thus, applied to the equations (18), the characteristic solutions are computed in the predictor stage of the FVC method as

$$\begin{aligned}
H^{n+1}_{i+1/2} &= \widetilde{H}^n_{i+1/2} - \frac{\Delta t}{\Delta x}\widetilde{H}^n_{i+1/2}\sum_{k=1}^{M} l_k\left(u^n_{k,i+1} - u^n_{k,i}\right), \\
Q^{n+1}_{k,i+1/2} &= \widetilde{Q}^n_{k,i+1/2} - \frac{\Delta t}{\Delta x}\Bigg(\widetilde{Q}^n_{k,i+1/2}\left(u^n_{k,i+1} - u^n_{k,i}\right) + g\widetilde{H}^n_{i+1/2}\Big(\left(H^n_{i+1} + B^n_{i+1}\right) - \left(H^n_i + B^n_i\right)\Big) + \\
&\qquad \frac{(\rho_s - \rho_w)}{2\widetilde{\rho}^n_{k,i+1/2}} g l_k\left(\widetilde{H}^n_{i+1/2}\right)^2\left(c^{n+1/2}_{i+1} - c^{n+1/2}_i\right)\Bigg), \\
P^{n+1}_{k,i+1/2} &= \widetilde{P}^n_{k,i+1/2} - \frac{\Delta t}{\Delta x}\widetilde{P}^n_{k,i+1/2}\left(u^n_{k,i+1} - u^n_{k,i}\right),
\end{aligned} \tag{24}$$

where $\widetilde{H}^n_{i+1/2} = H\left(t_n, X_{0,i+1/2}(t_n)\right)$, $\widetilde{Q}^n_{k,i+1/2} = Q_k\left(t_n, X_{k,i+1/2}(t_n)\right)$ and $\widetilde{P}^n_{k,i+1/2} = P_k\left(t_n, X_{k,i+1/2}(t_n)\right)$ are the solutions at the departure points $X_{k,i+1/2}(t_n)$ computed using the cubic Spline interpolation. To calculate the numerical fluxes $\mathbf{F}_{i\pm1/2} = \mathbf{F}\left(\mathbf{W}_{i\pm1/2}\right)$, the intermediate states $\mathbf{W}_{i\pm1/2}$ are updated using the characteristic solutions $\mathbf{U}_{i\pm1/2}$ in the predictor stage (24). Thus, using the first-order Euler scheme for illustration only, the solution in the FVC method (16) is obtained using the following corrector stage

$$\begin{aligned}
H^{n+1} &= H^n - \frac{\Delta t}{\Delta x}\sum_{k=1}^{M}\left(\left(l_k H u_k\right)^n_{i+1/2} - \left(l_k H u_k\right)^n_{i-1/2}\right), \\
Q^{n+1}_{k,i} &= Q^n_{k,i} - \frac{\Delta t}{\Delta x}\Bigg(\left(Hu^2_k + \frac{1}{2}gH^2\right)^n_{i+1/2} - \left(Hu^2_k + \frac{1}{2}gH^2\right)^n_{i-1/2}\Bigg) - \\
&\qquad \frac{\Delta t}{\Delta x} g\left(\widehat{H}^n_i\left(B^n_{i+1} - B^n_{i-1}\right) - \frac{(\rho_s - \rho_w)}{2\widehat{\rho}^n_{k,i}} l_k\left(\widehat{H}^n_i\right)^2\left(c^n_{k,i+1} - c^n_{k,i-1}\right)\right), \\
P^{n+1}_{k,i} &= P^n_{k,i} - \frac{\Delta t}{\Delta x}\left(\left(Hu_k c_k\right)^n_{i+1/2} - \left(Hu_k c_k\right)^n_{i-1/2}\right).
\end{aligned} \tag{25}$$

For the reconstruction of the terms $\widehat{H}^n_i$ and $\widehat{\rho}^n_{k,i}$, we use the same concept as in [4, 1] to guarantee that the discretization of the flux gradients and source terms in (16) are well balanced. Hence,

$$\widehat{H}^n_i = \frac{1}{4}\left(H^n_{i+1} + 2H^n_i + H^n_{i-1}\right), \qquad \widehat{\rho}^n_{k,i} = \frac{1}{4}\left(\rho^n_{k,i+1} + 2\rho^n_{k,i} + \rho^n_{k,i-1}\right). \tag{26}$$

Note that the discretization of equations (11) and (13) is straightforward and it is omitted here. It should also be mentioned that the considered FVC method is fully conservative by construction and the non-conservative system (17) is used only to compute the intermediate states for the numerical fluxes in (16).

4 Numerical results

In this section, we present the numerical results for a validation case and then for two test examples of a multi-layered dam-break problem over an erodible bed and a multi-layered wind-driven recirculation problem over a movable bed. The former is used to demonstrate the effects of the features added in this novel formulation, and the latter to demonstrate the recirculation and two-dimensional capabilities of the proposed model. We present results obtained using different numbers of layers in the flow domain, and we also investigate their impact on the erosion and deposition at the bed. It is expected that more layers used in the flow problem yield a smaller bottom velocity and consequently less erosion. In all our computations, the total water height H and total concentration C are given, and the water height h_k and concentration c_k at the kth layer are calculated using equal fractions as

$$h_k = l_k H, \qquad c_k = l_k C, \qquad \text{with} \qquad l_k = \frac{1}{M}, \qquad k = 1, \dots, M.$$

For the results presented in this section, the water density $\rho_w = 1000\ kg/m^3$ and the air density $\rho_a = 1.2\ kg/m^3$. Furthermore, a Courant number of $Cr = 0.85$ is used in our simulations and Δt is adjusted at each time step according to the stability condition

$$\Delta t = \mathrm{Cr} \frac{\Delta x}{\max\limits_{k=1,\dots,M} \left(\left|\lambda^n_{2,k}\right|, \left|\lambda^n_{3,k}\right|, \left|\lambda^n_{4,k}\right| \right)},$$

where $\lambda_{2,k}$, $\lambda_{3,k}$ and $\lambda_{4,k}$ are the eigenvalues of the single-layered sediment transport system given in (15). For a better presentation of the results we also generate two-dimensional velocity fields from our one-dimensional results using the post-processing procedure described in [1]. Thus, the vertical velocity w is computed from the divergence-free equation

$$\frac{\partial u}{\partial x} + \frac{\partial w}{\partial z} = 0. \tag{27}$$

Here, the vertical velocity w is recovered by integrating the equation (27) for each layer using non-penetration boundary conditions at the erodible bottom. The streamlines are also reconstructed from the two-dimensional velocity fields.

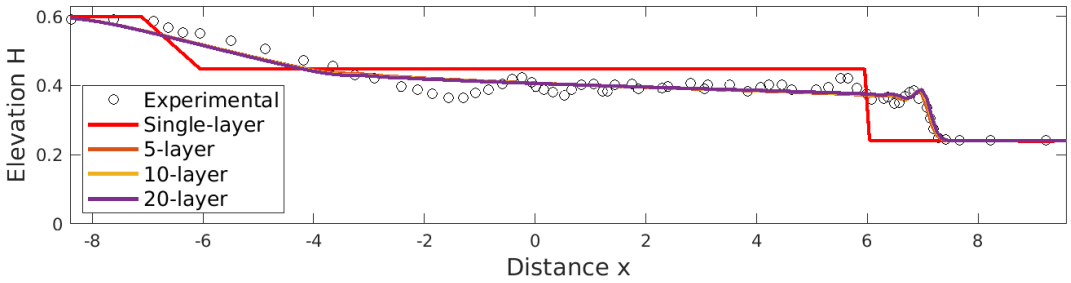

Figure 3: Comparison between experimental measurements and computational results obtained for the dam-break problem over a fixed bed at time $t = 3.5$ using different numbers of layers.

4.1 Dam-break problem over a fixed bed

In order to understand the effect of the multi-layer formulation on the erosion, we first consider the effect of the formulation on the evolution of the dam-break wave only. To this end, the experimental results presented in [18] are used as a benchmark problem for validation purposes. Here, a dam breaks over a flat fixed bed flume 19 m long. The initial conditions are given by

$$H(0,x) = \begin{cases} 0.6\ m, & \text{if} \quad x \leq 0, \\ \\ 0.24\ m, & \text{if} \quad x > 0, \end{cases} \qquad u_k(0,x) = 0\ m/s.$$

The dam-break is allowed to evolve up to a time $t = 3.5\ s$ after the dam breaks. The obtained results for the water elevation are shown in Figure 3 using different numbers of layers in the model a mesh with 100 gridpoints. As in [18], a reference solution obtained using the conventional single-layer shallow water equations is also included in this figure. It is clear from the computed solutions that the results obtained using the multi-layered model are in good agreement with the experimental measurements for this benchmark problem. Figure 3 also demonstrates the advantage of the multi-layer formulation and the effect of numbers of layers in the obtained results.

It is clear from the results presented in Figure 3 that the more accurate results are achieved by increasing the number of layers in the multi-layered model for this problem. For instance, using the 5-layer model in the simulations, the L^1 and L^2 errors are respectively 1.1126 and 0.1933 whereas using the 20-layer model these errors become 1.0669 and 0.1732, respectively. It also be noted that this increase in the accuracy is small, but it will become critical when evaluating a dam-break problem over movable bed as the water depth and velocity would be sensible to the erosion and deposition processes present in the model.

4.2 Dam-break problems over erodible beds

We consider a dam-break flow problem in a domain 50 m long and over flat erodible bed ($B(0,x) = 0$) and subject to the following initial conditions

$$H(0,x) = \begin{cases} 2\ m, & \text{if} \quad x \leq 0, \\ \\ 1\ m, & \text{if} \quad x > 0, \end{cases} \qquad C(0,x) = \begin{cases} 0.01, & \text{if} \quad x \leq 0, \\ \\ 0.001, & \text{if} \quad x > 0, \end{cases} \qquad u_k(0,x) = 0\ m/s.$$

The bed material is assumed to be a non-cohesive sand with density $\rho_s = 2650\ kg/m^3$, an average particle size of $d = 0.25\ mm$, an erosion coefficient of $\varphi = 0.015$, a critical shear stress of $0.0145\ Pa$, a porosity of $p = 0.4$, and a deposition coefficient of $w_s = 0.001$. The gravitational acceleration is set to $g = 9.81\ m/s^2$ and results are presented for different numbers of layers.

We first examine the performance of the proposed FVC method with respect to mesh and layer refinements. In Table 1 we summarize the obtained results using different numbers of layers M and different numbers of gridpoints N at time $t = 4\ s$. We present the minimum value of the bed profile $B_{\min}$, the horizontal location x_B for the minimum bed profile $B_{\min}$, the maximum bottom velocity $\max|u_1|$, the total sediment concentration, and the CPU times. It is clear that increasing the number of layers and/or the number of gridpoints results in an increase of the CPU time. However, the increase in the CPU times related to the increase of numbers of layers is minimal compared to the increase of numbers of gridpoints. Keeping the number of layers M fixed, the results obtained for the minimum value of the bed profile $B_{\min}$ and the maximum bottom velocity $\max|u_1|$ demonstrated a good convergence as the number of gridpoints N increases. The results obtained for the minimum bed profile $B_{\min}$ and for the total sediment concentration confirm that the number of layers has a

Table 1: Convergence results for the dam-break flow problem using different numbers of layers M and different numbers of gridpoints N at time $t = 4\ s$. Here, we list the minimum value of the bed profile B_{min}, the horizontal location x_B of $B_{\min}$, the maximum bottom velocity $\max|u_1|$, the total concentration, and the CPU times given in seconds.

M	N	$B_{\min}$	x_B	$\max\|u_1\|$	total c	CPU
5	50	-0.2402	0.4902	1.020	2.744	1.094
	100	-0.2433	0.2475	1.034	2.797	1.903
	200	-0.2439	0.1244	1.046	2.827	4.921
	400	-0.2435	0.0623	1.071	2.849	11.94
10	50	-0.2009	0.4902	0.9510	2.271	0.873
	100	-0.2033	0.2475	0.9714	2.290	1.894
	200	-0.2038	0.1244	0.9861	2.302	6.546
	400	-0.2036	0.0623	1.036	2.310	14.95
20	50	-0.1900	0.4902	0.9007	1.964	1.037
	100	-0.1892	0.2475	0.9180	1.902	2.579
	200	-0.1877	0.1244	0.9353	1.899	7.231
	400	-0.1881	0.0623	0.9864	1.900	17.15

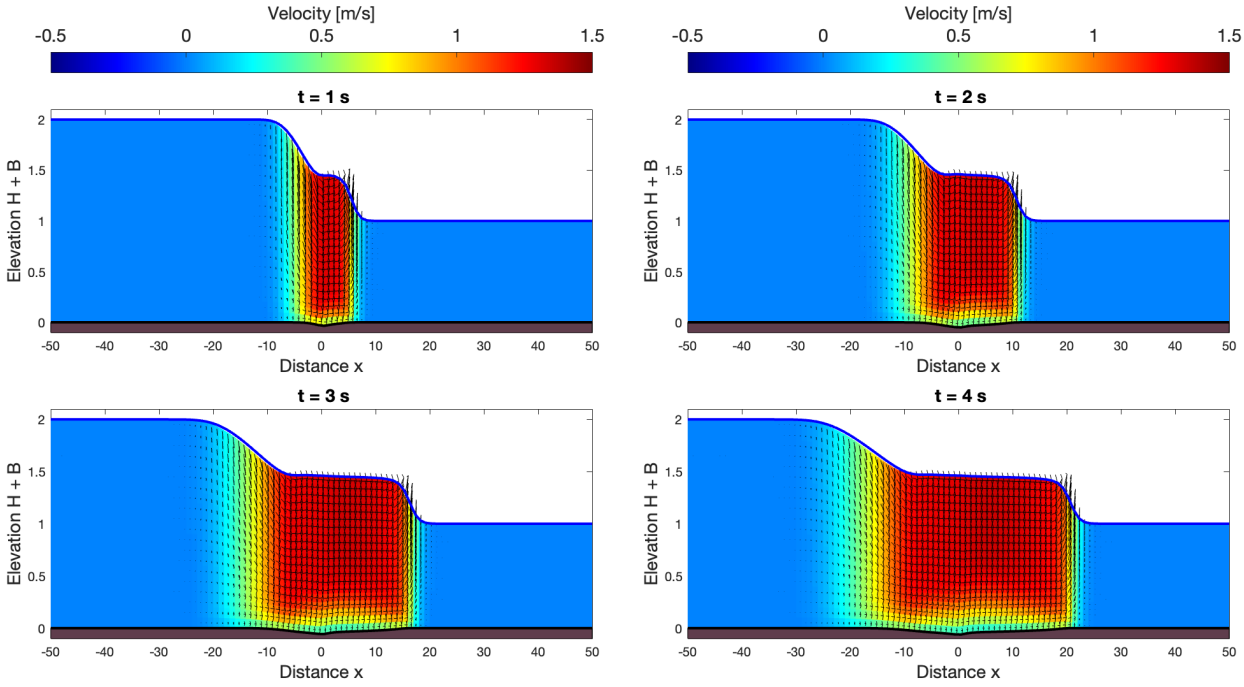

Figure 4: Velocity fields for the dam-break flow problem using 20 layers at four different instants. The colorbar refers to the intensity of the velocity fields.

profound impact on the sediment transport. Under the considered flow conditions, more layers in the system yield to lower bottom velocities and smaller total sediment concentrations.

In Figure 4 we present the water velocity and sediment concentration using 20 layers and 100 gridpoints at four different instants namely, $t = 1\ s$, $2\ s$, $3\ s$ and $4\ s$. In this figure the velocities are shown in two dimensions and it is clear to see the velocity gradient present in the lower layers which is the effect we set out to capture in this example. As in all dam-break flow problems, at $t = 0$ the dam collapses and the flow system consists of a shock wave traveling downstream and a rarefaction wave traveling upstream. As it can be seen from the results in Figure 4, no local undershoots or overshoots have been detected in the water velocity and the sediment concentration in the presence of steep gradients during the simulation process. The evolution of sediment concentrations shown in Figure 5 illustrates the sedimentary diffusion and profiles of the sediment concentration can clearly be seen diffusing up through the layers. Our FVC method accurately approximates the solution to this dam-break problem over the erodible bed. For instance, the qualitative comparison with similar numerical results reported in [3] for the single-layered counterpart of this test example is also satisfactory. The flow and sediment features are similar in both models but with differences in the magnitude of water velocity and the amount of erodible sediments in each model.

Figure 4 exhibits the velocity fields obtained using 20 layers and 100 gridpoints at times $t = 1\ s$, $2\ s$, $3\ s$ and $4\ s$. We also include in these figures the water free-surface and the profile of the erodible bed. The colorbars in these plots refer to the magnitude of the water velocities in the flow domain. As can be observed from these results, large horizontal velocities are generated in the area where the dam breaks and they propagate within the waterfronts. However, the vertical velocities within this area are weaker at the bottom layer compared to those obtained at the top layer. For the considered flow problem with 20 layers, the variation in the flow velocity creates a very active sediment exchange between the water flow and the bed load and also produces sharp spatial gradients in the sediment concentration. Overall the flow and the sediment features for this problem are recovered with no spurious oscillations appearing in the results obtained using the FVC method. Apparently, the computed results verify the stability and the shock capturing properties of the proposed FVC method. Here, Figure 5 also depicts the evolution of the concentrations across the layers and it demonstrates the bed material as passed up through the layers. It further demonstrates how the sedimentary distribution is heavily weighted towards the lower layers as discussed in [19] among others. As the flow ability to pick, deposit or retain sediment is mainly determined by its velocity, Figure 5 in conjunction with Figure 4 show the benefits of a multi-layered shallow water system when used for modelling sediment transport problems.

To check the effects of the number of layers on the bed-load and the sediment transport we display in Figure 6 the bed and velocity profiles obtained using the single-layered model and the multi-layered model with 2, 5, 10 and 20 layers. The results are presented at time $t = 4\ s$ using 100 gridpoints. Note that only the bottom velocity u_1 is used in the considered erosion formula (8) for the multi-layered simulations included in Figure 6. As expected, the single-layered model overestimates the bed velocity and more layers included in the multi-layered model yield smaller velocities near the bed. The results presented in Figure 6 for the velocity profiles also confirm the convergence in the considered multi-layered model such that, as the number of layers in the model increases the obtained velocity profiles are similar. Furthermore, as can be seen from the results in Figure 6, increasing the number of layers in the model results in a shallower erosion than the single-layered model which it is postulated overestimates the erosion. This effect is mainly due to the fact that larger number of layers in the multi-layered model yields to a small bottom velocity which in return is used for evaluating the erosion using the equation (8). It should also be stressed that we have observed no further improvements in results, not reported here, using a number of layers higher than 20. It is evident from the presented results that the dam-break flows over erodible sedimentary beds are highly affected by the number of layers in the model, such that the lower the number of layers the more significant bed erosion will be.

In Figure 7, we further examine the response of the sediment-load for the approximation of velocity in the erosion terms. Here, we plot the profiles of the bed using in the equation (8) the velocity obtained using the single-layered model, the multi-layered model with 20 layers, and the averaged velocity of the 20 layers. Again, using the water velocity obtained from the single-layered model or the averaged

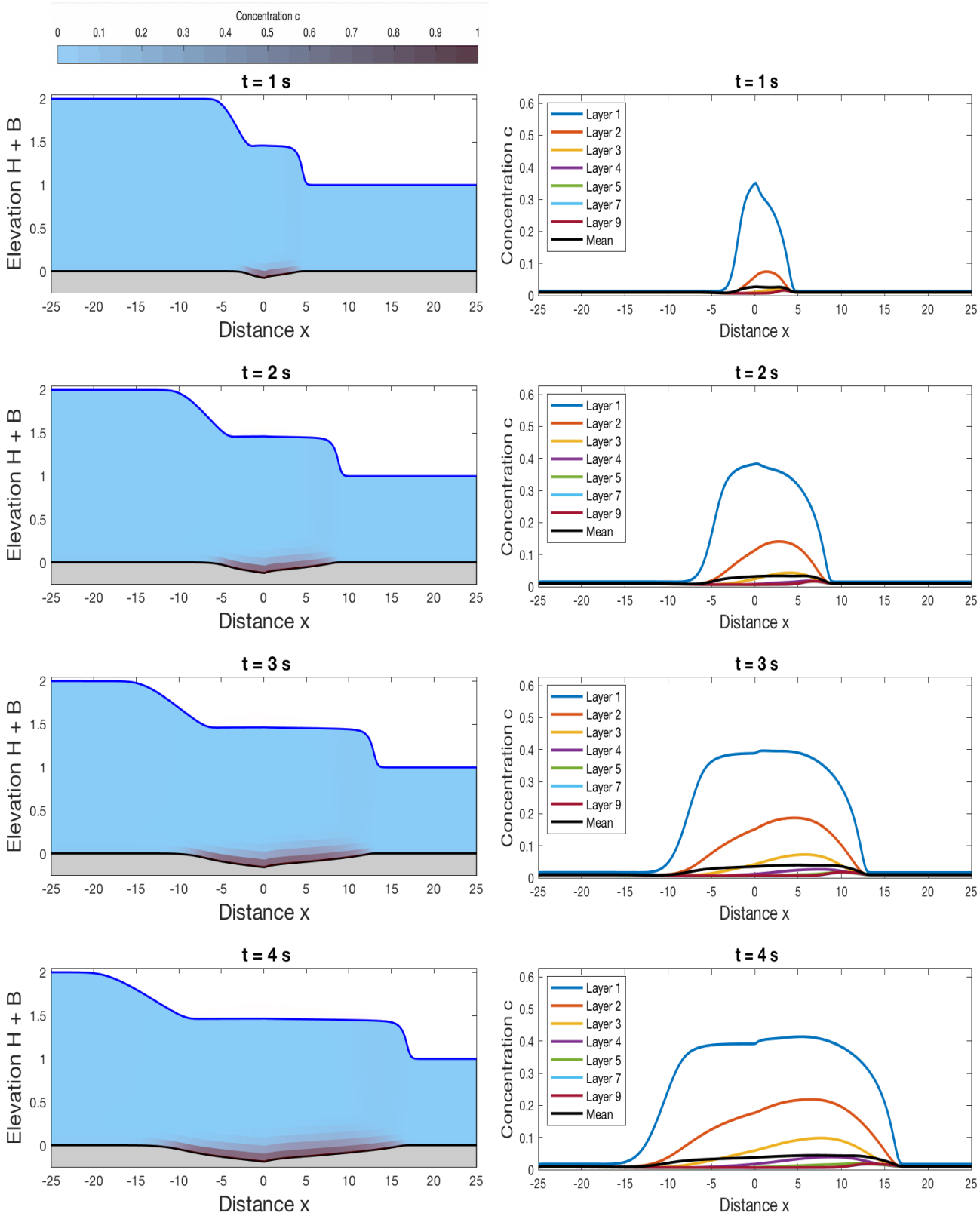

Figure 5: Sediment concentration (left column) and concentration profiles (right column) for the dam-break flow problem using 20 layers at four different instants. Only few selected layers are displayed.

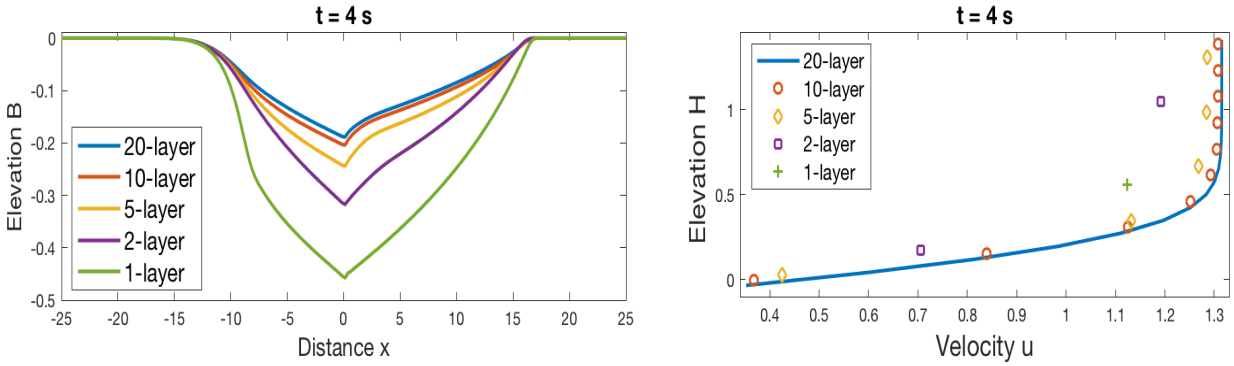

Figure 6: Bed profiles (left column) velocity profiles (right column) for the dam-break flow problem using different numbers of layers.

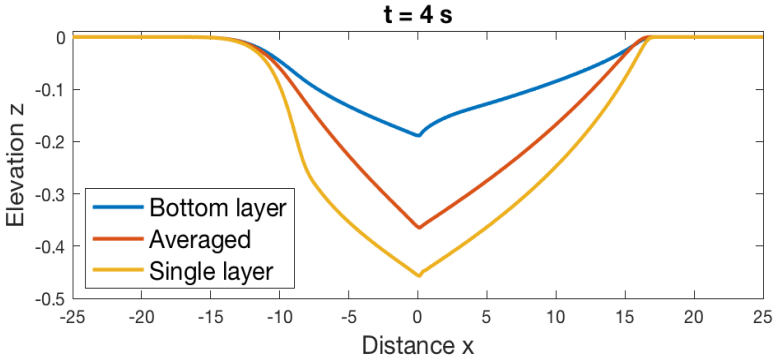

Figure 7: A comparison of bed profiles for the dam-break flow problem using different approximations of the velocity in the erosion term.

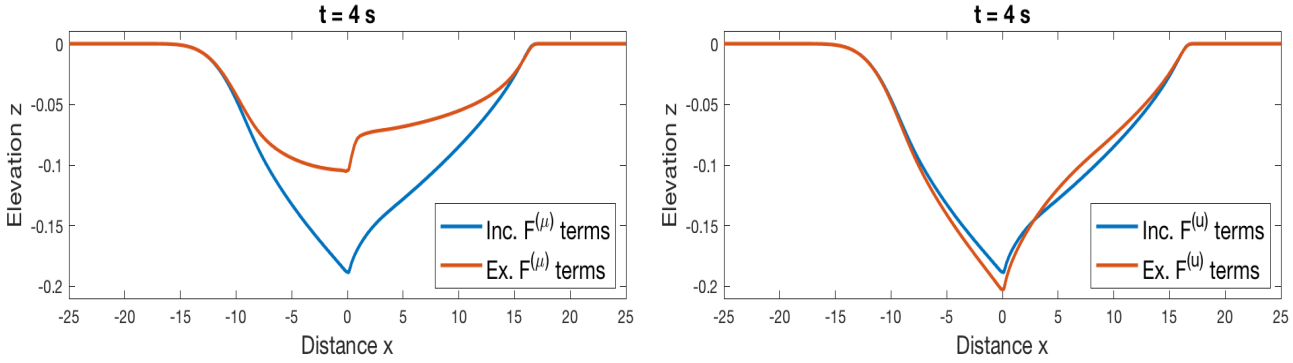

Figure 8: Bed profiles demonstrating the effect of the interlayer friction terms (left column) and the effect of the momentum exchange terms (right column) on the dam-break flow problem.

velocity from the multi-layered model in the erosion equations overestimates the real amount of the erosion in the sediment transport system. The results obtained using the bottom velocity from the multi-layered model with 20 layers seem to capture the correct sediment transport patterns. Note that, according to the erosion equation (8), an increase of the water velocity leads to an increase in the erosion effects. Thus, a weak erosion is expected for small near-bed velocity which is achieved

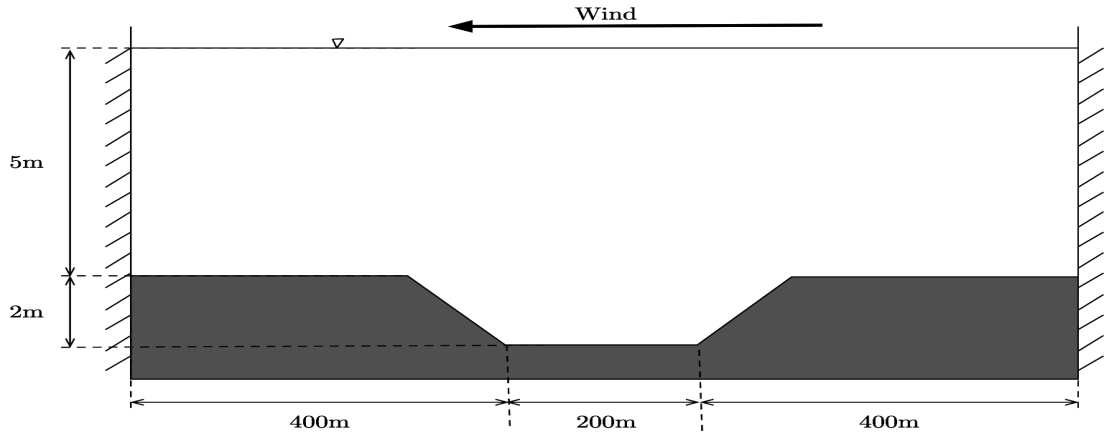

Figure 9: Illustration of the flow domain for the wind-driven recirculation problem over erodible beds.

very well using the multi-layered models.

Our final concern with this test example is to check the influence of the exchange terms in the multi-layered model (5) on the sediment transport results. To this end, we first solve the equations (5) without the mass exchange terms (*i.e.* $F^{(\mu)} = 0$) and with the mass exchange terms (*i.e.* $F^{(u)}$ defined in (10)). The obtained results for the water free-surface and the bed profile at time $t = 4\ s$ are illustrated in Figure 8. For the considered flow and sediment conditions, the effects of mass exchange terms on the morphological processes can be clearly seen on the bed profile. Observe the lack of erosion in the results without mass exchange terms compared to those obtained with mass exchange terms in Figure 8. The interlayer friction also has a smaller but noticeable effect on the bed-profile created. It is evident that accounting for mass exchange terms and interlayer friction in the multi-layered model modifies the near-bed velocity and it reproduces a well-developed sediment transport in the flow domain.

4.3 Wind-driven recirculation problems over erodible beds

In this example we consider a recirculation flow problem over a trench generated from a blowing wind on the surface. Here, the experiment is carried out in a rectangular channel containing a trench with 1:50 slopes as sketched in Figure 9. A similar domain has been studied in [11] for multi-layered shallow water equations in polydisperse sedimentation. The domain is 1 km long with a trench 2 m deep and 200 m long centered in the domain and subject to wind blowing from the left with a speed of 10 m/s and wind stress coefficient $\sigma^2 = 0.0015$. For the bed-load and suspended sediments we use the same sediment properties as in the previous test example for dam-break flows over erodible beds. Initially the flow is at rest and suspended sediments are injected in the trench at a depth below 3.5 m as

$$H(0,x) = 7\ m - B(0,x), \qquad C(0,x) = \begin{cases} 0.4, & \text{if} \quad 400\ m < x \leq 600\ m \quad \text{and} \quad -2\ m < z \leq 1.5\ m, \\ 0, & \text{elsewhere.} \end{cases}$$

It is worth remarking that in this example, the sediments are located only in a part of the computational domain $[400, 600]$ and only at a fixed water depth between $-2\ m$ and $1.5\ m$. This can not be implemented using a single concentration in the model and therefore, it justifies the inclusion of multiple concentrations c_k in our multi-layered system (5). Here, the concentration $c_k(0,x) = 0.4$ for $x \in [400, 600]$ and for each layer k located at a depth between $z = -2\ m$ and $z = 1.5\ m$. Note that, unlike the previous flow problem over erodible beds, the water flow in the considered problem is very

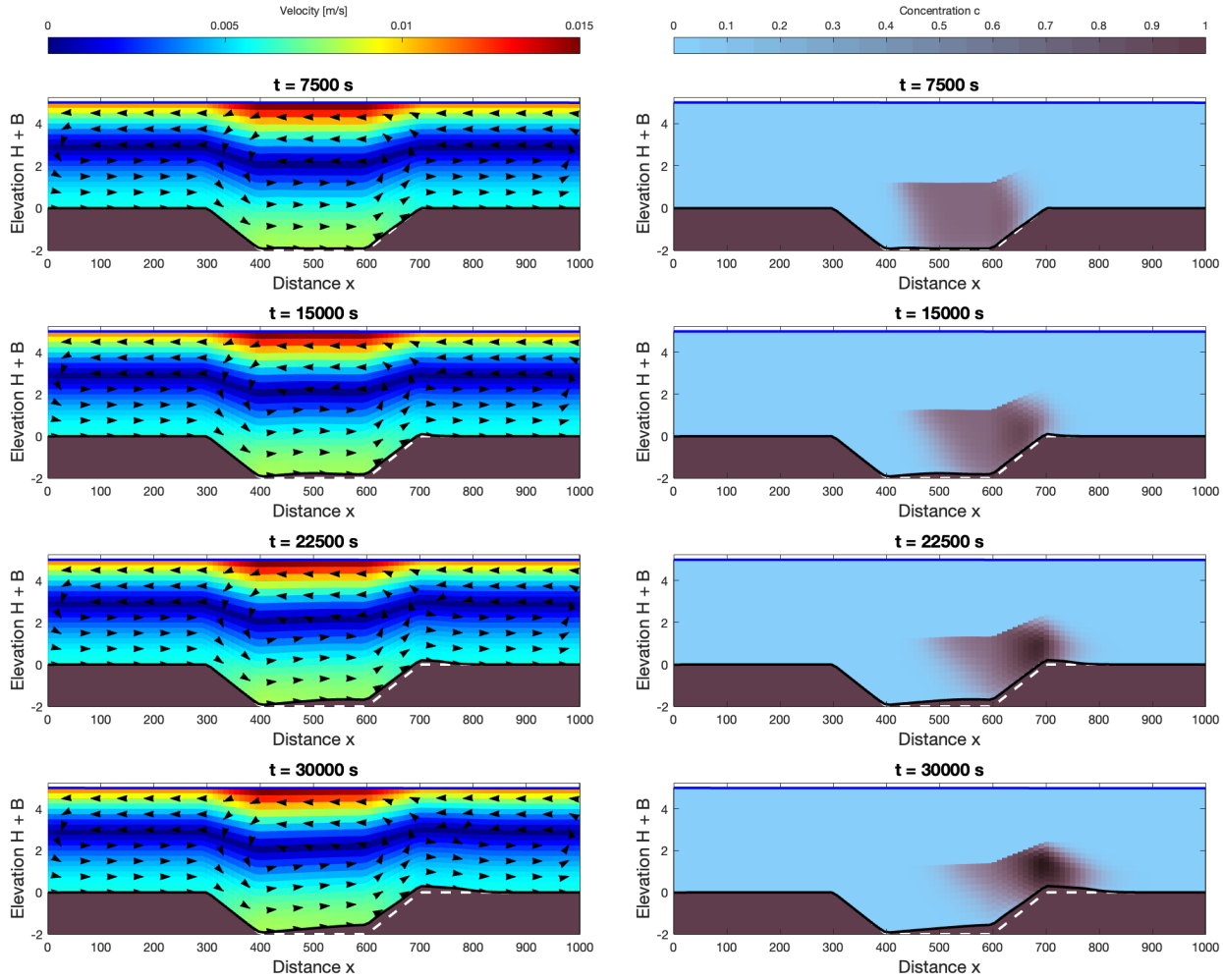

Figure 10: Velocity field (left column) and sediment concentration (right column) for the wind-driven recirculation problem using 20 layers at four different instants. The dashed line indicates the initial bed profile. Colorbars indicate the velocity intensity (left) and sediment concentration (right), and streamlines are shown on the velocity plot (left).

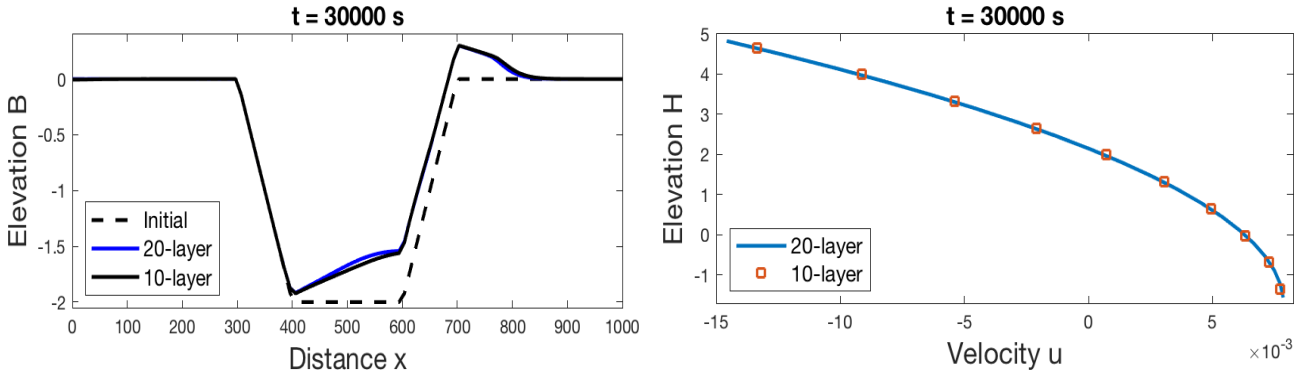

Figure 11: Bed profiles (left column) velocity profiles (right column) for the wind-driven recirculation problem using 10 and 20 layers.

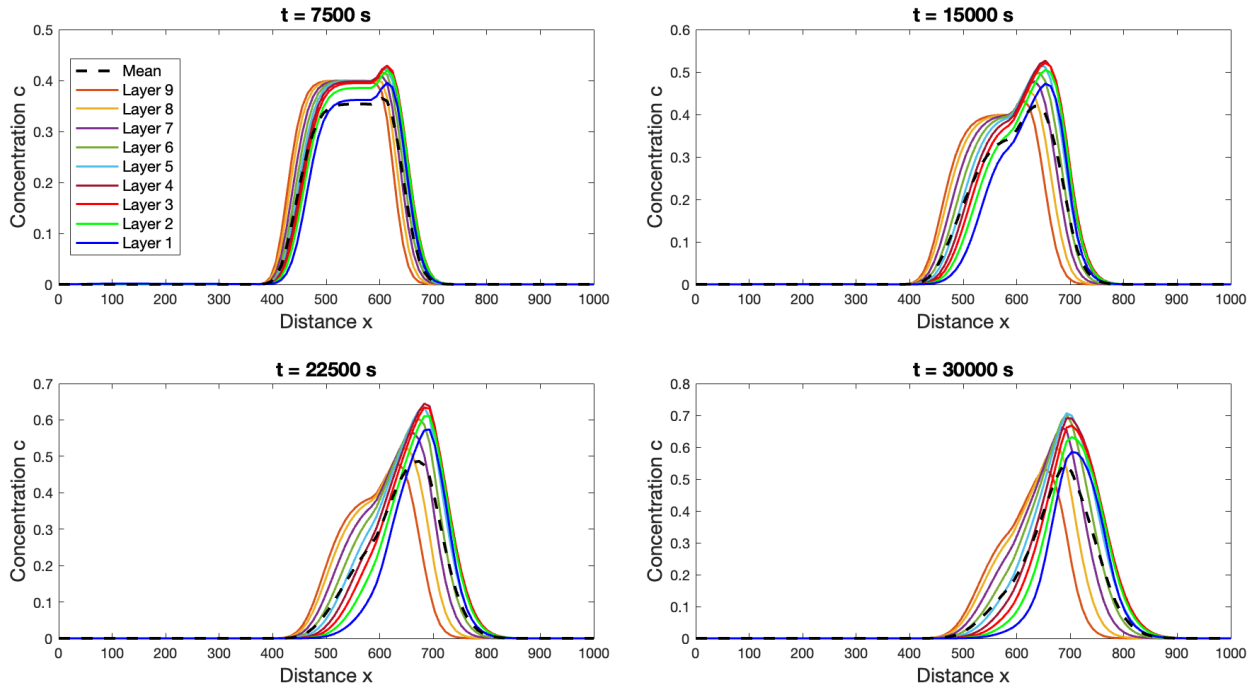

Figure 12: Sediment concentration for the wind-driven recirculation problem using 10 layers (left column) and 20 layers (right column) at four different instants. Only few selected layers are displayed.

slow and the morphodynamical problem with movable bed resulting in the formation of deposition and weak shocks. Therefore, a good numerical accuracy is required in order to capture the different phenomena present in its evolving solution. As a consequence, the later flow problem over erodible beds is more difficult to handle but the results shown here illustrate the robustness of the proposed FVC method. For all results presented in this section, the computational domain is discretized in 100 gridpoints and flow velocities, bed profiles and sediment concentrations are shown for 10-layered and 20-layered models at four different times $t = 7500\ s$, $15000\ s$, $22500\ s$ and $30000\ s$. Notice that these large times are required in the simulation for the water flow to build up speeds and generate recirculations in the domain as well as some dynamics at the bed.

The results obtained using 20 layers are presented in Figure 10. For this test example, the water free-surface remains relatively flat during the simulation times however, the velocity fields and sediment concentrations exhibit different flow and sediment features. Observe the recirculation zones appeared in the velocity fields obtained using the 20-layered models. Due to the structure of the channel topography, a strong inner recirculation is generated at the center of the domain with a weaker outer recirculation near the domain walls. Obviously, large values of the water velocity are located on the top layer as it can be seen in the snapshots of the velocity intensities in Figure Figure 10. It is also observed that due to the inner recirculation slightly high velocities are created in the flow domain. The proposed FVC method performs well for this unsteady multi-layered flow problem and it produces accurate numerical solutions without requiring special treatment of the source terms or complicated upwind discretizations of the gradient fluxes in the multi-layered equations.

Now, we turn our attention to the sediment transport associated with this problem. Note that in this problem we use a non-natural concentration distribution as set out in the initial conditions. As can be seen from the results for the sediment concentrations in Figure 10 for the 20-layered models, the suspended sediments form a plume which is advected by the water flow in the opposite direction to the wind force. As demonstrated in the results, the inter-layer diffusion terms (10) are crucial to

this model as sediments are able to transit between layers and retain normality. Note that these flow and sediment features are impossible to recover using the conventional single-layered model studied for example in [5, 7, 3].

Under the actual flow conditions, the erosion is negligible and the deposition is the dominant factor in this test example. This is essentially attributed to the water velocity created at the bottom layer near the bed. To emphasis this features we illustrate in Figure 11 the bed and the vertical velocity profiles obtained using the 10-layered and 20-layered models. The vertical velocity profiles in the model exhibit a decrease in the velocity from the top layer at the free-surface to the bottom layer near the bed. There are very little differences between the bed profiles in the 10-layered and 20-layered models. For visualizing the comparisons, we display in Figure 12 the sediment concentrations obtained using the 10-layered model and the 20-layered model at the four selected simulation times. Comparing the mean concentrations in these results, we can see a difference in the amplitudes between the 10-layered and 20-layered results. For the considered flow and sediment conditions, a convergence in terms of number of layers in the model is achieved using 20 layers. Again, the FVC method performs well for this wind-driven recirculation problem over erodible beds since it does not dissipate the moving fronts and no nonphysical oscillations have been observed when the water flows over the trench. It should also pointed out that the performance of our FVC method is very attractive since the computed solutions remain stable and oscillation-free even for coarse grids without solving nonlinear systems or Riemann problems.

5 Conclusions

In this study we have presented a new model that combines the multi-layered shallow water equations with the sediment transport including erosion and deposition effects. Mass exchange terms are accounted for in the inter-layered coupling for both water flow and sediment transport as well as including vertical sediment diffusion. To solve the coupled system, we have implemented the finite volume characteristics method along with a second-order splitting to deal with the source terms. The finite volume characteristics method is second-order accurate and it consists of two stages which can be viewed as a predictor-corrector procedure. In the first stage, the method reconstructs the numerical fluxes using the method of characteristics. This stage results in an upwind discretization of the characteristic variables and avoids the Riemann problem solvers. In the second stage, the solution is updated using the finite volume discretization of the conservation system. The method combines the attractive attributes of the finite volume discretization and the method of characteristics to yield a simple solver for multi-layered shallow water flows over erodible beds. The proposed method exhibited good shape, high accuracy and stability behavior for all sediment transport regimes considered. Verification of the proposed method has been carried out by first using a benchmark problem to compare the obtained results to experimental data and demonstrate the effect of number of multi-layers on the computed results, and next by using a test example of dam-break flows over erodible beds and a test example of wind-driven recirculation flows over movable beds. The presented results demonstrate the capability of the multi-layered models that can provide insight to complex suspended sediment and bed-load transport in free-surface flows. The extension of the proposed multi-layered models to the two-dimensional sediment transport problems will be the topic of future research.

Data Availability Statement

The data underlying the results can be obtained from the corresponding author on reasonable request.

References

[1] E. Audusse, F. Benkhaldoun, S. Sari, M. Seaid, and P. Tassi. A fast finite volume solver for multi-layered shallow water flows with mass exchange. *Journal of Computational Physics*, 272:23–45, 2014.

[2] E. Audusse, M. Bristeau, M. Pelanti, and J. Sainte-Marie. Approximation of the hydrostatic Navier-Stokes system for density stratified flows by a multilayer model: kinetic interpretation and numerical solution. *J. Comput. Phys.*, 230:3453–3478, 2011.

[3] F. Benkhaldoun, S. Sari, and M. Seaid. A flux-limiter method for dam-break flows over erodible sediment beds. *Applied Mathematical Modelling*, 36:4847–4861, 2012.

[4] F. Benkhaldoun and M. Seaid. A simple finite volume method for the shallow water equations. *J. Comp. Applied Math.*, 234:58–72, 2010.

[5] Z. Cao and P. Carling. Mathematical modelling of alluvial rivers: Reality and myth. part I: General overview. *Water Maritime Engineering*, 154:207–220, 2002.

[6] Z. Cao and G. Pender. Numerical modelling of alluvial rivers subject to interactive sediment mining and feeding. *Advances in Water Resources*, 27:533–546, 2004.

[7] Z. Cao, G. Pender, S. Wallis, and P. Carling. Computational dam-break hydraulics over erodible sediment bed. *Journal of Hydraulic Engineering*, 67:149–152, 2004.

[8] L. Chumakova, F. Menzaque, P. Milewski, R. Rosales, E. Tabak, and C. Turner. Shear instability for stratified hydrostatic flows. *Communications on Pure and Applied Mathematics*, 62:183–197, 2009.

[9] P. Dyke. *Modeling Costal and Offshore Processes*. Imperial College Press, 2007.

[10] H. A. Einstein. Formulas for the transportation of bed load. *Transactions of the American Society of Civil Engineers*, 107:561–573, 1949.

[11] E. Fernández-Nieto, E. Koné, T. Morales de Luna, and R. Burger. A multilayer shallow water system for polydisperse sedimentation. *Journal of Computational Physics*, 238:281–314, 2013.

[12] E. Fernández-Nieto, E. Koné, and Chacón T. A multilayer method for the hydrostatic Navier-Stokes equations: A particular weak solution. *J. Sci. Comput.*, 57:1–30, 2013.

[13] A. Grass. Sediment transport by waves and currents. *SERC London Cent. Mar. Technol.*, FL29, 1981.

[14] J. Gula, V. Zeitlin, and F. Bouchut. Instabilities of buoyancy-driven coastal currents and their nonlinear evolution in the two-layer rotating shallow water model. Part 2. Active lower layer. *J. Fluid Mechanics.*, 665:209–237, 2010.

[15] J. Guo and P. Y. Julien. Turbulent velocity profiles in sediment-laden flows. *J. of Hydraulic Research*, 39(1):11–23, 2001.

[16] S. Huang, Z. Sun, D. Xu, and S. Xia. Vertical distribution of sediment concentration. *Journal of Zhejiang University SCIENCE*, 9(11):1560–1566, 2008.

[17] E. Kubatko and J. Westerink. Exact discontinuous solutions of Exner bed evolution model: simple theory for sediment bores. *Journal of Hydraulic Engineering*, 133(3):305–311, 2007.

[18] W. Liu, B. Yunliang, W. Chao, and L. Xin. Assessing the analytical solution of one-dimensional gravity wave model equations using dam-break experimental measurements. *Water*, 10(9), 2018.

[19] X. Liu. New Near-Wall Treatment for Suspended Sediment Transport Simulations with High-Reynolds Number (HRN) Turbulence Models. *J. Hydaul. Eng*, 140:333–339, 2014.

[20] X. Liu, A. Mohammadian, and J. Sedano. A numerical model for three-dimensional shallow water flows with sharp gradients over mobile topography. *Computers & Fluids.*, 154:1–11, 2017.

[21] E. Meyer-Peter and R. Müller. Formulas for bed-load transport. *Report on 2nd meeting on international association on hydraulic structures research*, pages 39–64, 1948.

[22] T. Rowan and M. Seaid. Efficient computational models for shallow water flows over multilayer erodible beds. *Engineering Computations*, 37:401–429, 2019.

[23] T. Rowan and M. Seaid. Two-dimensional numerical modelling of shallow water flows over multilayer movable beds. *Applied Mathematical Modelling*, 88:474–497, 2020.

[24] W. W. Rubey. Settling velocity of gravel, sand, and silt particles. *American Journal of Science*, 148:325–338, 1933.

[25] C.W. Shu. Total variation diminishing time discretizations. *SIAM J. Sci. Stat. Comput.*, 9:1073–1084, 1988.

[26] H. Smaoui and F. Boughanim. 1D vertical model for suspended sediment transport in turbulent tidal flow: Application to the English Channel. *Computers & Geosciences*, 33:1111–1129, 2007.

[27] K. Terzaghi, R. B. Peck, and G. Mersi. *Soil Mechanics in Engineering Practice.* John Wile & Sons Publishers, 1996.

[28] L. C. Van Rijn. Unified view of sediment transport by currents and waves. I: Initiation of motion, bed roughness, and bed-load transport. *Journal of Hydraulic Engineering*, 113:649–667, 2007.

[29] V. A. Vanoni and G. N. Nomicos. Resistance properties of sediment-laden streams. *Transactions of the American Society of Civil Engineers*, 125(1):1140–1167, 1960.

[30] K. Vercruysse, R.C. Grabowski, and Rickson R.J. Suspended sediment transport dynamics in rivers: Multi-scale drivers of temporal variation. *Earth-Science Reviews*, 166:38–52, 2017.

[31] Z. B. Wang, R. J. Fokkink, and A. Langerak. A dynamic-empirical model for estuarine morphology. In *Physics of Estuaries and Coastal Seas*, pages 279–286, Balkema, Rotterdam, 1998.

[32] W. Wu and S. S. Wang. Formulas for sediment porosity and settling velocity. *Journal of Hydraulic Engineering*, 132:858–862, 2006.

[33] Z. Yang, Z. Zou, W. Xue, and D Sun. Experimental study of near-bed concentration and sediment vertical mixing parameter for vertical concentration distribution in the surf zone. *International Journal of Sediment Research*, 35:27–41, 2020.

[34] S. Zhao, J. Ovadia, X. Liu, Y.T. Zhang, and Q. Nie. Operator splitting implicit integration factor methods for stiff reaction-diffusion-advection systems. *J. Comput. Physics*, 230:5996–6009, 2011.